BULLETIN OF THE POLISH ACADEMY OF SCIENCES
TECHNICAL SCIENCES, Vol. 74(2), 2026, Article number: e157567
DOI: 10.24425/bpasts.2026.157567

Performance, sizing, and residual load – an analysis of photovoltaic systems for a water treatment facility

Thomas LIBERSKI[1]*, **Fausto A. CANALES**[1,2], **and Jakub JURASZ**[1]

[1] Faculty of Environmental Engineering, Wroclaw University of Science and Technology, 50-370 Wroclaw, Poland
[2] Civil Engineering Program, Faculty of Engineering, Sede Campus Nueva Granada, Universidad Militar Nueva Granada, Cajicá 250247, Colombia

Abstract. This study presents an analysis of photovoltaic (PV) systems designed for a water supply utility located in the Lower Silesian Voivodeship, Poland, focusing on system sizing, configurations, and residual load implications. The analysis has two key objectives: maximizing the capacity factor and self-consumption and then comparing both cases using residual load. Using hourly electricity demand data from eight locations, along with satellite-based solar irradiance and weather inputs, the research identifies optimal tilt and azimuth configurations under both objectives. The findings reveal that capacity factor optimization yields annual capacity factor values ranging from 13.00% to 13.38%, but results in lower self-consumption rates (ranging from 33.39% to 46.59%). In contrast, self-consumption optimization produces higher levels (ranging from 35.11% to 47.39%) but leads to reduced capacity factor performance (ranging from 6.93% to 11.57%). A centralized PV system configuration is also evaluated, achieving a capacity factor of 13.27% and self-consumption of 42.08% in the capacity factor optimized case, and 6.93% capacity factor with 44.84% self-consumption in the self-consumption optimized case. The results highlight a trade-off between maximizing energy yield and improving temporal matching of generation and demand, with each optimization strategy enhancing a different aspect of PV system performance in electricity supply for the critical infrastructure operation.

Keywords: solar power systems; renewable energy; sustainable water supply systems; energy droughts; decentralized electricity supply; PV orientation optimization.

1. INTRODUCTION

The rising costs of conventional energy sources have propelled the integration of photovoltaic (PV) systems into water treatment plants, as pointed out by Świętochowski *et al.* [1]. In Chabour *et al.*, it is stated that water and wastewater facilities consume a substantial amount of electrical energy, accounting for a significant portion of global energy consumption (4%), with the energy footprint of the urban water cycle ranging from 0.21 to 4.07 kWh/m^3 [2]. According to benchmarking data from the Polish Chamber of Waterworks and Sewerage, in 2017, the average energy intensity of water supply processes was around 0.65 kWh/m^3 [3]. As environmental regulations and water quality standards are tightened, the implementation of advanced treatment processes requiring significant energy inputs becomes unavoidable, and consequently, the incorporation of PV systems offers a compelling strategy for mitigating the rising energy expenditures and lowering the environmental impact within water treatment facilities, as stated by Douville & Macknick [4]. Zhao *et al.* note that PV systems have emerged as a promising solution for reducing the reliance on traditional centralized energy supplies, decreasing energy costs, and lowering greenhouse gas emissions in water distribution systems [5].

*e-mail: thomas.liberski@pwr.edu.pl

Manuscript submitted 2025-07-02, revised 2025-12-30, initially accepted for publication 2026-01-01, published in March 2026.

2. LITERATURE REVIEW

The operation of water distribution systems, which are essential for delivering water to residential, commercial, industrial, and agricultural consumers, demands substantial energy, requiring power for various processes such as pumping, aeration, filtration, and disinfection [5]. Pumping itself accounts for approximately 80% of the total energy consumption in water treatment facilities [5]. As pointed out by Stawowy *et al.*, this is especially relevant for energy-intensive subsystems of water provision and treatment, such as water treatment facilities, where operators must consider both the cost and the sustainable, low-carbon-emitting source of energy [6].

2.1. Photovoltaic systems in water treatment plants

To address the need for environmentally friendly operation, Collivignarelli *et al.* highlight that increasing attention has been given to implementing processes that ensure the quality of treated wastewater and protect the environment [7]. Bartecka *et al.* state that hybrid energy systems based on renewable energy sources, such as PV systems and wind turbines, can play a significant role in reducing greenhouse gas emissions [8]. The integration of PV systems into water treatment plants presents an opportunity to address critical environmental and economic challenges, aligning with the global pursuit of sustainable development and resource management [9, 10]. Since solar PV technology may lead to reduced energy prices and greenhouse gas emissions, it has emerged as the most appealing renew-

able energy source option for powering water treatment plants, according to Shao *et al.* [11]. Their analysis shows that, depending on the weather, the electricity consumption of the plant declined by 59.2%, 50.2%, and 33.8%, while carbon emissions connected to electricity decreased by 47.5%, 37.3%, and 25.0%, respectively [11]. These systems can be employed for both central and decentralized water treatment, according to Szpak *et al.* [12]. Cooperation with PV systems can benefit water storage tanks and even entire water treatment plants by providing electricity independent of external power sources during electricity shortages, showing the compatibility of renewable energy technologies and water infrastructure [12].

2.2. Energy yield optimization

To maximize the benefits of PV systems implemented in water treatment facilities, it is essential to optimize their energy yield by adjusting installation parameters. Sreewirote *et al.* state that optimizing the energy yield of PV systems involves careful consideration of installation parameters, such as azimuth and tilt angle, which directly influence the amount of solar radiation captured by the panels and, consequently, the electricity generated [13]. Kazanecka & Olczak note that Poland's latitudinal position (49°00′ to 54°50′ N) affects seasonal solar irradiance due to changes in solar elevation, causing fluctuations in PV yield. Solar radiation peaks in the summer and drops in the winter, requiring careful selection of the tilt angle to balance seasonal variations. Single-sided PV systems achieve maximum yield at tilt angles of 20°–45°, with lower angles favoring summer energy and steeper angles improving winter output, which is particularly relevant in the Northern Hemisphere [14]. In addition to solar positioning, another key factor is the soiling of PV modules. Steeper tilt angles reduce dirt accumulation and facilitate natural cleaning by wind and rainfall, reducing performance losses compared to flatter surfaces [15]. Jaszczur *et al.* find that in most cases, the power output delivered by the modules decreases due to dust accumulation [16]. Borah *et al.* report that the highest PV energy loss occurred at a 0° tilt angle, and that it decreased progressively with higher tilt angles [15]. Cano *et al.* state that modules set at low tilt angles (below 15°) tend to retain water on their surfaces after rainfall, the water combines with dust, forming a sticky substance that cannot be removed by wind [17]. Finally, the azimuth angle, which defines the orientation of the panel with respect to true north, also plays a crucial role in energy yield optimization, with south-facing orientations preferred in the Northern Hemisphere to capture maximum sunlight throughout the day [1].

2.3. Capacity factor

A metric related to energy yield is the capacity factor (CF). CF is calculated by dividing the actual energy output of the PV system over a period, usually a year, by the energy it would have produced if it had operated at its rated power output continuously during the same period [18]. In this context, CF serves as a performance indicator, allowing for comparison between configurations.

2.4. Self-consumption considerations

In addition to maximizing total energy yield, increasing the amount of electricity consumed directly on-site, known as self-consumption (SC), is becoming an important aspect of PV system design, as it reduces grid dependency. González-Morán *et al.* provide a definition of SC, or auto-consumption, and refer to it as electricity generated by prosumers for their own use, thereby lowering their reliance on the distribution network [19]. Nyholm *et al.* define SC as the portion of locally consumed PV electricity that is not exported to the grid, calculated as the lower value between electricity demand and the sum of PV generation and battery discharge [20]. There is growing interest among grid-connected PV system owners in enhancing their SC rate [21]. For water treatment plants, aligning PV energy generation with on-site electricity demand is vital for maximizing SC. A key factor positively affecting SC is the size (installed power capacity) of the PV array [22]. Another aspect of SC is the rapidly growing number of PV installations, and increasing the SC value has become critical, as it helps mitigate the risk of overloading the distribution network [21]. A practical example of renewable energy use in a water utility is Wodociągi Chrzanowskie (located in southern Poland, Lesser Poland Voivodeship), which has achieved an SC rate of over 27% across all operations. One of its sublocations is powered by a 19.58 kWp PV array that supplies approximately 50% of its annual electricity demand [23]. SC is not the only necessary metric that should be considered when designing PV systems; another aspect to consider is the residual load (RL). In today's changing climate, the possibility of low PV generation events is another topic that should be investigated. RL is a relevant metric when assessing PV systems, as it reflects the limitations of solar generation during low output periods and indicates the potential role of complementary energy sources in maintaining supply continuity.

2.5. Residual load implications

RL is defined as the difference between energy demand and total renewable energy production [24]. Positive RL (PRL) is the share of electricity demand unmet by renewable energy sources and supplied by conventional generation [25]. Minimizing PRL is essential for ensuring grid stability and reducing the need for conventional power resources [19]. Extreme PRL events occur when demand exceeds renewable output, often during weather events such as anticyclones that reduce wind and solar generation while coinciding with high loads [26]. Such events should be considered when analyzing PV systems. Understanding the RL profile is crucial for assessing the potential for energy droughts. For the scope of this research, energy droughts are defined as periods when electricity demand exceeds available supply, potentially leading to power outages or disruptions in water treatment operations. Literature about an RL analysis in the context of energy droughts performed for a single facility is scarce, and such an analysis has never been conducted for a water utility in Poland. Based on the literature review above, the following research questions have been formulated:

1. Does the orientation (azimuth and tilt angle settings) of a PV installation, maximizing energy yield, also maximize self-consumption in the analyzed water treatment facility?

2. Can a centralized PV system effectively meet the aggregated energy demand of a multi-site water treatment facility, and how does it compare to decentralized configurations?
3. What are the implications of RL, and how do they relate to a low-energy generation event?

3. METHODOLOGY

To investigate the research questions presented above, this study analyzes a specific case involving a multi-site water treatment facility located in a city within the Lower Silesian Voivodeship, in the southwestern region of Poland. The analysis is based on energy load data with an hourly resolution collected from nine locations within the water utility network, consisting of five pump stations and four water treatment plants. At Location 3, one electricity meter supplies two subsystems consisting of two pump stations; therefore, in this study, these two pump stations are treated as a single location. Consequently, eight distinct locations form the basis of the analysis conducted. All the sublocations of this facility and the distances between them are shown in Fig. 1.

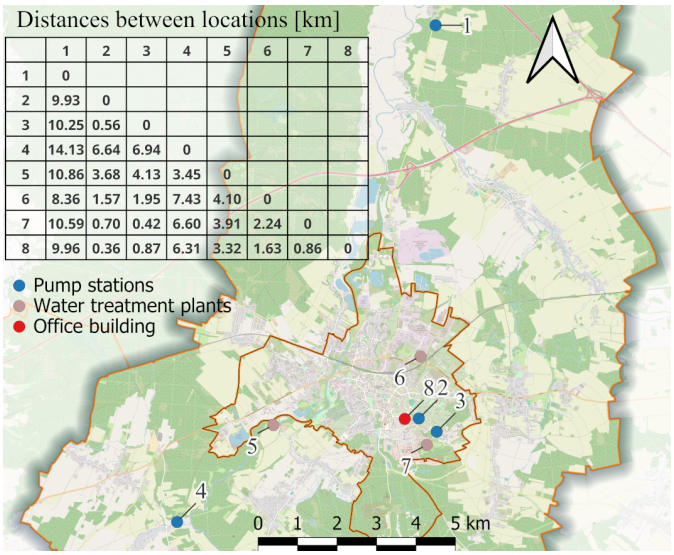

	1	2	3	4	5	6	7	8
1	0							
2	9.93	0						
3	10.25	0.56	0					
4	14.13	6.64	6.94	0				
5	10.86	3.68	4.13	3.45	0			
6	8.36	1.57	1.95	7.43	4.10	0		
7	10.59	0.70	0.42	6.60	3.91	2.24	0	
8	9.96	0.36	0.87	6.31	3.32	1.63	0.86	0

Fig. 1. Locations of water supply system components and distances between them (Location 8 functions as both an office facility and a backup water treatment plant)

Locations 1–4, which are pump stations, account for more than one-third of the annual water volume across all eight sites. In the case of pump stations, water volume refers solely to the volume of water pumped at those locations. The pumped water volume at the pump stations is dominated by Location 3, which accounts for more than 80% of the total volume of all pump stations, whereas Locations 1, 2, and 4 each contribute only single-digit percentages. As far as water treatment plants are concerned, Location 5 accounts for approximately 37% of the annual water volume, Locations 6 and 7 each contribute about 13%, while Location 8 provides only a marginal share (around 1%). Location 8 is a backup facility, which only supports the rest of the water treatment plants. In the case of water treatment plants, the water volume refers to water pumped and treated, ready to be delivered as potable water to the network. Figure 2 shows all the percentages and volumes of water at each location.

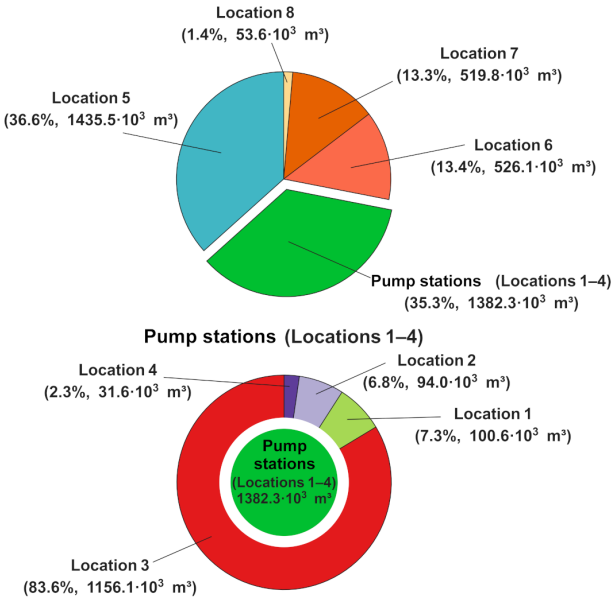

Fig. 2. Annual volume of treated and pumped water for a given facility type

The Satellite Application Facility on Climate Monitoring Surface Solar Radiation Data Set – Heliosat, Version 3.0 (CM SAF SARAH-3.0) is used, with hourly resolution in watts per square meter across all locations [27]. In addition, temperature data in kelvin and wind data in meters per second are obtained from the European Centre for Medium-Range Weather Forecasts Fifth Generation of Atmospheric Reanalyzes (ECMWF ERA5), with both datasets available at hourly resolution for all locations [28]. These meteorological inputs are processed using a MATLAB-based PV generation model that simulates hourly PV energy output for azimuth angles ranging from eastward to westward orientation, and tilt angles from 10° to 90°. The PV generation model assumes a 1 kilowatt-peak (kWp) PV array at each site. A minimal tilt angle of 10° was introduced to avoid flat installed modules, which are hard to model due to soiling effects [15]. Using this data and considering an annual energy constraint where annual PV generation equals annual energy demand, the analysis identifies the optimal tilt and azimuth angles for each location under CF and SC optimization scenarios. In both scenarios, a centralized PV system configuration is also considered, using an aggregated load profile constructed by summing the hourly demand across all locations. To evaluate the feasibility of a centralized PV, the correlation of PV generation across sites is analyzed using configurations calculated for CF and SC optimized cases. Finally, an RL analysis at daily and hourly resolutions is performed for both the CF and SC optimized cases, including their centralized configurations. The whole methodology is outlined in Fig. 3, which provides a schematic overview of the workflow. It summarizes the key steps, starting from data input, followed by PV generation modeling, output data collection, and concluding with the assessment of CF, SC, and RL.

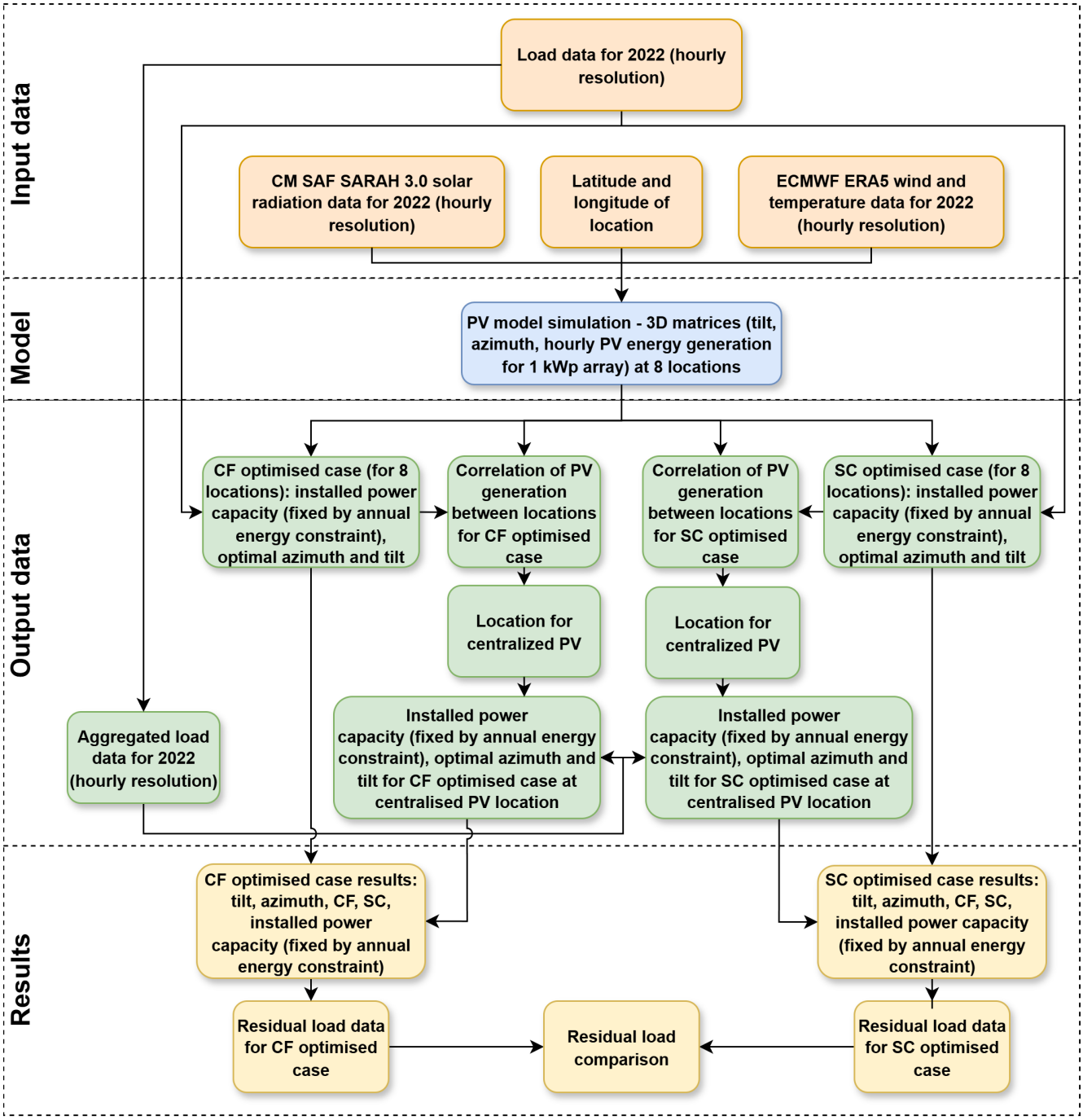

Fig. 3. The methodology applied in this research

The MATLAB model developed for this study simulates the hourly power output of PV systems using the previously mentioned meteorological inputs. These are paired with geographic coordinates (latitude and longitude) for each location. For every hour of the year, the model calculates the Sun's position using solar declination, hour angle, zenith angle, and azimuth angle, followed by the angle of incidence on the tilted PV surface. It then derives the beam, diffuse, and reflected radiation components and uses them to compute the total irradiance on the panel surface. Based on this irradiance, combined with ambient conditions, the model estimates the PV module temperature and corrects efficiency accordingly. It then calculates hourly power output, accounting for temperature effects and system losses. This process is repeated for all combinations of candidate tilt angles (10–90°) and azimuth angles (−90° to +90°), where −90° is east, 0° is south, and 90° is west. The increment for both tilt and azimuth angles is 1°. Finally, the results are stored in 3D matrices representing PV generation for each tilt and azimuth configuration for a standardized 1 kWp PV system. The model is described in detail in Fig. 4 [29–39].

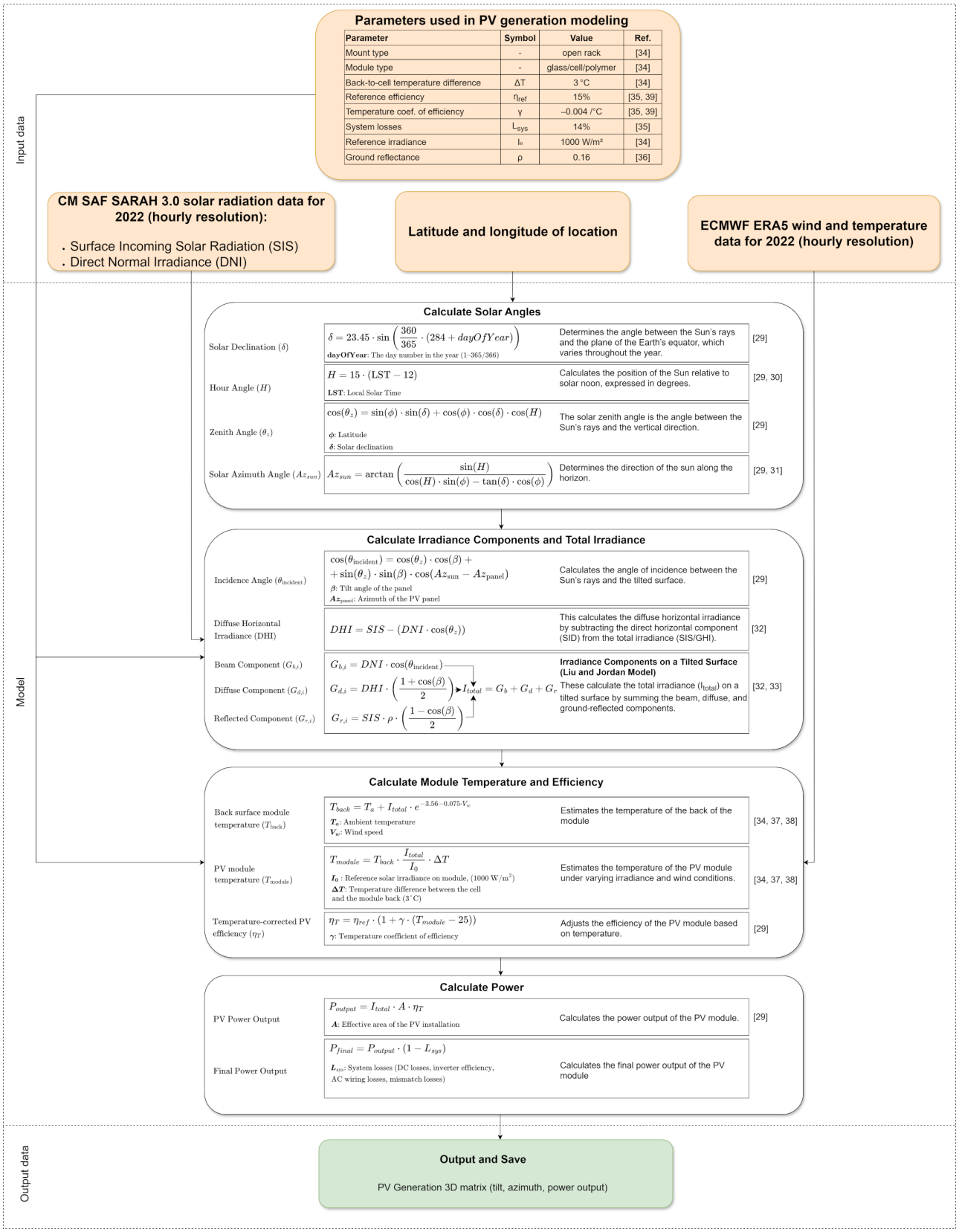

Fig. 4. Methodological flowchart for the PV generation model encompassing: solar angle calculations (adapted from [29–31]), irradiance components and total irradiance (adapted from [29,32,33]), module temperature and efficiency (adapted from [29,34,37,38]), power calculations (adapted from [29]) and key physical and empirical parameters used in PV performance modeling (taken from [34–36, 39]). The reference efficiency, temperature coefficient of efficiency and system losses parameters used in this model were specifically chosen for the lower bound of today's standard ranges to ensure generality and applicability across a wide variety of PV module types

3.1. Capacity factor calculations

The calculation aims to determine the optimal tilt and azimuth angles for each location to achieve the highest CF and, additionally, the required installed power capacity of the PV system (in kWp), to meet the annual energy demand, which is the sum of all the hourly demands. The CF is calculated using the basic formula shown in equation (1):

$$\mathrm{CF} = \left(\frac{E_{\mathrm{gen}}}{8760 \times P_{\mathrm{rated}}} \right) \times 100, \tag{1}$$

where E_{gen} is the annual energy output in kilowatt-hours, P_{rated} is the installed power capacity of the rated system in kWp, and 8760 is the total number of hours in a year. In this approach, tilt angles and azimuths are selected individually for each location to maximize energy yield, as shown in equation (2):

$$(\theta^*, \phi^*) = \arg\max_{\theta,\phi} \left(\frac{E_{\mathrm{gen}}(\theta,\phi)}{8760 \times P_{\mathrm{rated}}} \times 100 \right), \tag{2}$$

where θ^* is the optimal tilt angle, ϕ^* is the optimal azimuth angle, $E_{\mathrm{gen}}(\theta,\phi)$ is the annual energy output in kilowatt-hours at tilt θ and azimuth ϕ, P_{rated} in this case is fixed at 1 kWp, the CF is thus calculated for all orientations using a normalized 1 kWp PV system, and $\arg\max_{\theta,\phi}$ is the operator that returns the tilt and azimuth pair that maximizes the capacity factor.

The next step is to calculate the actual installed power capacity ($P_{\mathrm{rated}}(\theta,\phi)$) at the optimal tilt and azimuth to meet the annual energy demand, which is achieved by using the formula in equation (3):

$$P_{\mathrm{rated}}(\theta,\phi) = \frac{E_{\mathrm{demand}}}{E_{\mathrm{gen}}(\theta,\phi)}, \tag{3}$$

where E_{demand} is the total annual energy demand in kilowatt-hours and $E_{\mathrm{gen}}(\theta,\phi)$ is the annual energy output from a 1 kWp system at tilt θ and azimuth ϕ also in kilowatt-hours.

3.2. Self-consumption calculations

The SC optimization is performed individually for each location. In this approach, the tilt and azimuth angles of the PV system are selected to maximize the SC ratio, based on the specific load profile of each site. For every orientation, the PV system is scaled so that the annual energy generation exactly matches the annual energy demand. This ensures that all orientations are evaluated under equal energy supply conditions. The optimal tilt and azimuth are identified using the following criterion, shown in equation (4):

$$(\theta^*, \phi^*) = \arg\max_{\theta,\phi} \left(\frac{E_{\mathrm{self}}(\theta,\phi)}{E_{\mathrm{gen}}(\theta,\phi)} \right), \tag{4}$$

where θ^* and ϕ^* are the optimal tilt and azimuth angles, respectively, $E_{\mathrm{self}}(\theta,\phi)$ is the total annual energy in kilowatt-hours, directly self-consumed at a given orientation, and $E_{\mathrm{gen}}(\theta,\phi)$ is the total annual energy generated by the scaled PV system at the same orientation also in kilowatt-hours. The operator $\arg\max_{\theta,\phi}$ selects the orientation that maximizes the SC ratio. To ensure the requirement is fulfilled, the required installed power capacity of the system, $P_{\mathrm{rated}}(\theta,\phi)$ at each orientation, is calculated as in equation (3).

After scaling the system, self-consumed energy is computed as:

$$E_{\mathrm{self}}(\theta,\phi) = \frac{1}{1000} \sum_{t=1}^{8760} \min\left(P_{\mathrm{PV}}(t;\theta,\phi), P_{\mathrm{demand}}(t) \right), \tag{5}$$

where $P_{\mathrm{PV}}(t;\theta,\phi)$ is the scaled PV output, and $P_{\mathrm{demand}}(t)$ is the hourly power demand, both in watts at hour t. The element-wise minimum ensures that only the energy consumed directly by the load is counted. The sum is taken over all hours in the year and divided by 1000 to convert watt-hours to kilowatt-hours. The total generated energy at each orientation is computed analogously to equation (6):

$$E_{\mathrm{gen}}(\theta,\phi) = \frac{1}{1000} \sum_{t=1}^{8760} P_{\mathrm{PV}}(t;\theta,\phi), \tag{6}$$

where $P_{\mathrm{PV}}(t;\theta,\phi)$ is the power output of the PV system in watts at hour t, based on the specific tilt θ and azimuth ϕ.

The summation captures the total annual energy produced by the PV system over the year. The result is divided by 1000 to convert from watt-hours to kilowatt-hours, yielding the total annual energy generation $E_{\mathrm{gen}}(\theta,\phi)$ in kilowatt-hours for the given orientation.

3.3. Centralized PV system for aggregated load

For both the CF and SC maximization approaches, a single PV installation is considered to serve an aggregated load. The aggregated-load PV system is adopted because of potential advantages in terms of economies of scale and simplified management. The aggregated load is calculated by summing the whole energy demand in a year. The location for such a system was selected based on a comprehensive evaluation of a range of factors, including land availability for infrastructure and the energy demands of individual sites. Figure 5 shows the distribution of annual energy demand for each location. Location 5 was chosen as the site for the centralized PV system because of the land availability and the large share of energy demand. Energy demands of pump stations are much smaller than those of the water treatment plants and are shown on the lower chart of Fig. 5.

To evaluate the potential of an aggregated PV system, several characteristics of PV systems must be considered. One relevant feature is spatial smoothing, which describes how the combined power output of separate plants becomes more stable as the distance between them increases. This can be analyzed by examining how the correlation between sites decreases with distance (decorrelation/smoothing effect) [40]. The Pearson correlation coefficient was calculated after omitting hours during which PV generation was zero at all locations (night hours), and the calculations were performed for both CF and SC optimized cases, as shown in Table 1.

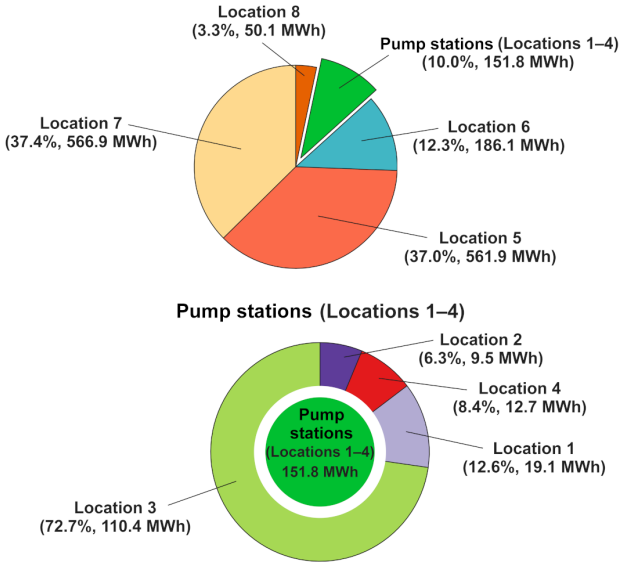

Fig. 5. Distribution of total annual load across locations

Table 1
Pearson correlation coefficient for PV generation (upper triangle for CF optimized case, lower triangle for SC optimized case)

Location	1	2	3	4	5	6	7	8
1	–	0.98	0.97	0.96	0.97	0.98	0.97	0.98
2	0.91	–	1.00	0.97	0.99	1.00	1.00	1.00
3	0.83	0.68	–	0.97	0.99	1.00	1.00	1.00
4	0.81	0.66	0.96	–	0.99	0.97	0.97	0.98
5	0.83	0.67	0.97	0.99	–	0.99	0.99	0.99
6	0.97	0.91	0.88	0.85	0.87	–	1.00	1.00
7	0.83	0.68	1.00	0.96	0.97	0.88	–	1.00
8	0.88	1.00	0.64	0.62	0.63	0.88	0.64	–

The Pearson correlation coefficients exhibit extremely high values for the CF optimized case, ranging from 0.96 to 1.00. This indicates that as the geographic distance between locations increases, the similarity in PV generation profiles decreases. Although the correlation coefficients decrease with distance in the CF optimized case, the PV correlation coefficients are still high between all locations, showing the viability of a centralized PV system. In the SC optimized case, the results present a broader range, from 0.62 to 1.00. This variation arises because Locations 1, 2, 6, and 8 have different PV system orientation results compared to the other locations, which will be discussed later in Section 4.2. This also implies that spatial distance does not meaningfully explain the variability in PV generation correlation across sites. In this case, the viability of a centralized PV system is worse than in the CF optimized case, primarily because the correlation of PV generation is worse between locations with lower power demand (Pump stations and Location 8) and locations with high power demand, such as Locations 5, 6, and 7. The centralized PV system will be considered in later calculations.

3.4. Residual load calculations

The RL represents the difference between the power demanded by the load and the power supplied by the PV system at each hour. It indicates how much additional energy must be covered by external sources, such as the electrical grid, when the PV generation is insufficient to meet the instantaneous demand [24]. For each location, the RL is calculated on an hourly basis, considering the PV configurations for both the CF and SC optimized cases. The RL for each location and optimization case is determined using the formula shown in equation (7):

$$\mathrm{RL}(t) = P_{\mathrm{dem}}(t) - P_{\mathrm{PV}}(t), \tag{7}$$

where $\mathrm{RL}(t)$ is the RL in watts at time t, $P_{\mathrm{dem}}(t)$ is the power demand in watts at time t and $P_{\mathrm{PV}}(t)$ is the PV generation in watts at time t. An analysis at daily and hourly resolution is conducted.

Because the analysis is conducted for a water supply utility, where certain locations experience periods of zero load (such as Location 7 for multiple weeks), special considerations are made in the RL calculations. If the power demand is zero and the PV generation at the same time is also zero, the RL percentage is defined as 100%, indicating that the full demand remains unmet. This reflects the presence of unavoidable auxiliary and standby electricity consumption (e.g., control systems, monitoring, and metering equipment) that is not captured in the reported load data. Conversely, if the power demand is zero while the PV generation is greater than zero, the RL percentage is defined as 0%, reflecting that although energy was produced, there was no significant demand to consume it. Those special considerations are described in equation (8):

$$\mathrm{RL}\,\% = \begin{cases} 100, & \text{if } P_{\mathrm{dem}} = 0 \wedge P_{\mathrm{PV}} = 0, \\ 0, & \text{if } P_{\mathrm{dem}} = 0 \wedge P_{\mathrm{PV}} > 0, \\ \dfrac{P_{\mathrm{dem}} - P_{\mathrm{PV}}}{P_{\mathrm{dem}}} \times 100 & \text{if } P_{\mathrm{dem}} > 0. \end{cases} \tag{8}$$

To evaluate the potential occurrence of energy droughts, the RL is analyzed for each PV system configuration. This analysis helps in identifying periods of heightened vulnerability, allowing for an assessment of potential resilience against energy drought events.

4. RESULTS

In this study, the results provide insight into the performance of PV systems across multiple water treatment and pumping sites, with particular focus on PV installed power capacity, CF, SC, and RL under varying orientation configurations. The analysis identifies optimal tilt and azimuth angles for both CF and SC optimized cases at each site and evaluates both decentralized and centralized PV scenarios.

4.1. CF optimized case

The results for the CF optimized case, including the optimal tilt and azimuth angles, PV capacity, and corresponding SC rates for each location, are presented in Table 2.

Table 2
Results for the CF optimized case

Location	Tilt	Azimuth	CF	PV capacity	SC
1	34°	−7°	13.00%	16.81 kWp	39.94%
2	34°	−6°	13.35%	8.14 kWp	40.53%
3	34°	−6°	13.37%	94.29 kWp	40.26%
4	34°	−6°	13.28%	10.96 kWp	43.82%
5	34°	−6°	13.27%	483.52 kWp	43.41%
6	34°	−6°	13.30%	159.8 kWp	33.39%
7	34°	−6°	13.38%	483.8 kWp	41.05%
8	34°	−6°	13.34%	42.91 kWp	46.59%
Centralized PV	34°	−6°	13.27%	1305.4 kWp	42.08%

Table 3
Results for the SC optimized case

Location	Tilt	Azimuth	CF	PV capacity	SC
1	38°	90°	10.16%	21.5 kWp	41.99%
2	14°	90°	11.46%	9.48 kWp	41.30%
3	90°	90°	6.97%	180.97 kWp	43.04%
4	90°	90°	6.95%	20.91 kWp	46.36%
5	90°	90°	6.93%	925.84 kWp	46.37%
6	42°	90°	10.20%	208.29 kWp	35.11%
7	90°	90°	6.97%	928.09 kWp	43.43%
8	10°	90°	11.57%	49.45 kWp	47.39%
Centralized PV	90°	90°	6.93%	2499.5 kWp	44.84%

All locations achieve maximum generation performance at a consistent tilt angle of 34°, with minor azimuth variations from −7° to −6° (relative to South), reflecting a south-facing orientation with slight eastward adjustment. CF across sites is uniform, ranging from 13.00% to 13.38%, indicating similar solar resource availability and system performance.

The highest CF is at Location 7 (13.38%), and the lowest is at Location 1 (13.00%). A comparable performance level was observed by Gulkowski, who reported an average annual yield of 990.2 kWh/kWp (equivalent to a CF of approximately 13.4%) for PV systems in south-eastern Poland [41]. PV system capacities vary significantly based on demand (Fig. 5), from 8.14 kWp at Location 2 to 483.8 kWp at Location 7. SC rates range between 33.39% and 46.59%, the highest at Location 8 and the lowest at Location 6. The centralized PV configuration, based on an aggregated load, has a total capacity of 1305.4 kWp, a CF of 13.27%, and an SC of 42.08%. This performance is comparable to the decentralized setup, suggesting that centralization does not significantly compromise system efficiency and could offer benefits in terms of management and scalability. This also implies that centralization could simplify maintenance and reduce installation costs without significant efficiency trade-offs.

4.2. SC optimized case

The results for optimizing PV configurations in the context of maximizing SC across the analyzed locations are presented in Table 3.

Compared to the CF optimized scenario, the tilt angles are significantly steeper, in most cases being 90°. Only for locations 1, 2, 6, and 8, the tilt angles are noticeably lower, while azimuth angles (measured relative to South) are in all cases 90°, which is west. This positioning shifts generation away from solar noon towards the evening hours, improving overlap with demand profiles and enhancing SC. Despite lower CF across all sites, ranging from 6.93% to 11.57%, the SC rates are higher than in the CF optimized case. The reduced CF is an expected trade-off, as the generation profile is skewed to better match load rather than to maximize total energy production. System capacities range from 9.48 kWp at Location 2 to 928.09 kWp at Location 7. The centralized PV configuration for the aggregated load results in a system rated at 2499.5 kWp, with a CF of 6.93% and an SC of 44.84%. This supports the feasibility of centralization from an SC perspective, albeit with a significant trade-off in CF.

4.3. Residual load results

For the CF optimized cases, PV generation peaks sharply around solar noon, reflecting orientations aimed at maximizing daily energy output. While this maximizes yield, it often causes midday overproduction and negative RL (NRL) during peak sunlight. In contrast, the SC optimized cases shift generation toward the afternoon, better aligning with typical demand and reducing production-consumption mismatch. This shift is especially clear at Locations 3, 4, 5, and 7, where afternoon RL peaks are more pronounced than in CF cases. At Locations 2 and 8, lower tilt angles in the SC optimized case yield an RL profile extremely close to the one from the CF case. Figure 6 shows average daily power profiles across all locations and a centralized PV setup, highlighting afternoon-weighted generation of SC cases. For this figure, hourly demand data and PV generation data were used to calculate mean demand and RL values for every hour of a day.

For further analysis of RL, an approach based on PV deployment levels is used. The PV deployment levels ranging from 75% to 100% are selected to reflect the expected 25-year operational lifespan of standard PV modules, incorporating a simulated 1% annual decline in energy generation efficiency [42]. The analysis of the daily RL for the CF optimized case, examined at a daily resolution across varying PV deployment levels and days of the year for each location and the centralized PV configuration, reveals a consistent trend. Specifically, during the high-irradiance summer period (days 150–250), a marked overgeneration occurs. At full PV deployment, all locations experience sustained daily NRL, driven by high solar availability and system sizing optimized for maximum annual yield. The most extreme daily summer NRL occurs at Location 6 (–256.1%), Location 8 (–236.0%), and Location 2 (–160.7%), indicating substantial oversupply relative to demand on peak days. Even at a reduced PV level deployment of 75%, daily summer RL falls well be-

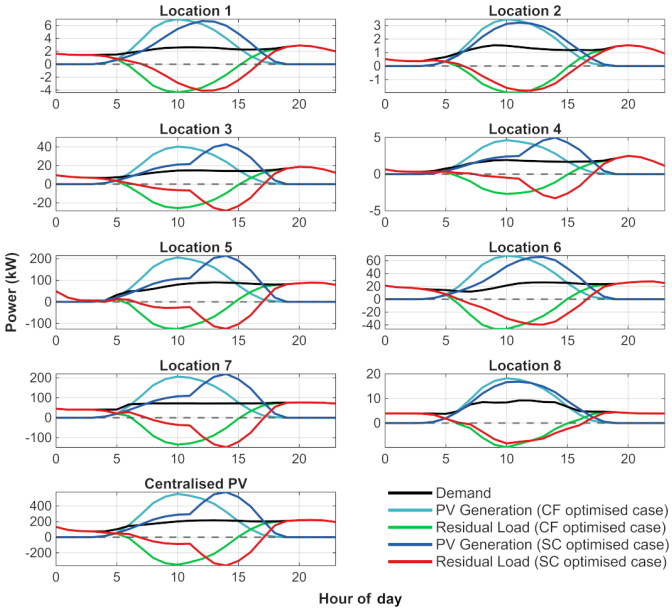

Fig. 6. Comparison of average daily profiles for demand, PV generation, and RL for the CF and SC optimized cases

low zero across most locations, with values such as –167.1% at Location 6, –152.0% at Location 8, and –95.5% at Location 2. Over the full year, RL remains negative, demonstrating that the overgeneration extends beyond summer peaks. The daily NRL values also often span multiple consecutive days, forming prolonged periods of excess energy supply. These NRL values often exceed 100% of the local energy demand, highlighting the scale of surplus generation from the PV systems at each location. The proposed centralized PV system serving an aggregated load also exhibits substantial overgeneration. At full PV deployment, it reaches a minimum daily summer NRL of–108.9% and a daily yearly minimum NRL of –128.9%. All the above findings are illustrated in Fig. 7a, which also visually suggests that PV deployment levels do not significantly alter the overall RL dynamics in the CF optimized case for all the locations and the centralized PV system for the aggregated load. In Fig. 7, hourly demand, and PV generation data (with PV deployment ranging from 75 to 100%) were used to calculate mean RL values for every day in a year.

In the SC optimized case, the RL analysis at a daily resolution reveals that overgeneration remains a consistent feature across all locations, similar to the CF optimized case, particularly during the high-irradiance summer period (days 150–250). At full PV deployment, the most extreme daily summer NRL values are recorded at Location 8 (–279.1%), Location 6 (–269.6%), and Location 2 (–201.0%), highlighting significant oversupply relative to demand on peak days. Even at 75% deployment, daily summer NRL still reaches –184.3% at Location 8, –177.2% at Location 6, and –125.7% at Location 2. These NRL values frequently span multiple consecutive days, forming prolonged periods of surplus generation. The centralized PV system serving an aggregated load also reflects this pattern, with a minimum daily summer NRL of –147.1% at full deployment and –85.3% at 75% deployment. When comparing both the CF and SC optimized cases directly, the SC optimized case results in even lower minimum daily NRL at nearly all locations, suggesting that surplus generation is not inherently reduced by aligning PV output more closely with demand profiles. Instead, the optimization for SC may shift peak production to slightly earlier or later hours without significantly mitigating seasonal mismatches. Comparison of the SC and CF optimized cases reveals that the three largest changes in minimum daily NRL between configurations occur

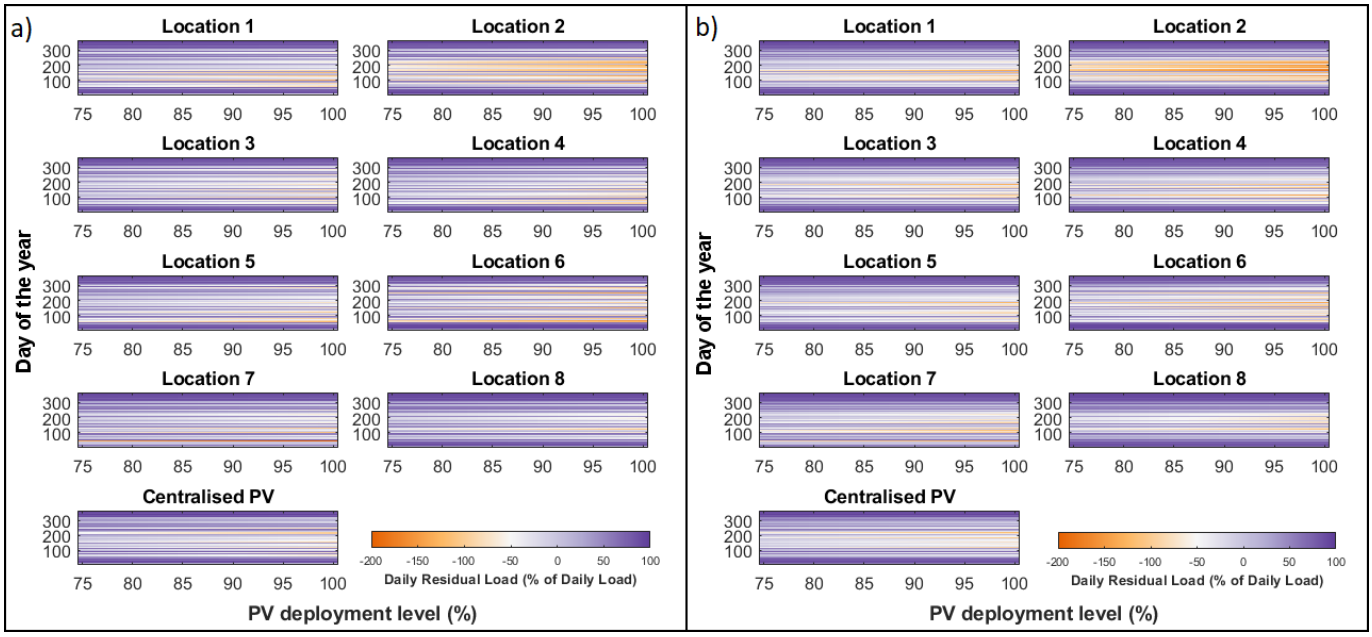

Fig. 7. Daily RL for the CF optimized case (a) and SC optimized case (b) across PV deployment levels for each location and the centralized PV system (the values presented here follow a similar approach for showing RL and PV deployment levels presented in [25]). Daily RL values are capped at –200% for readability

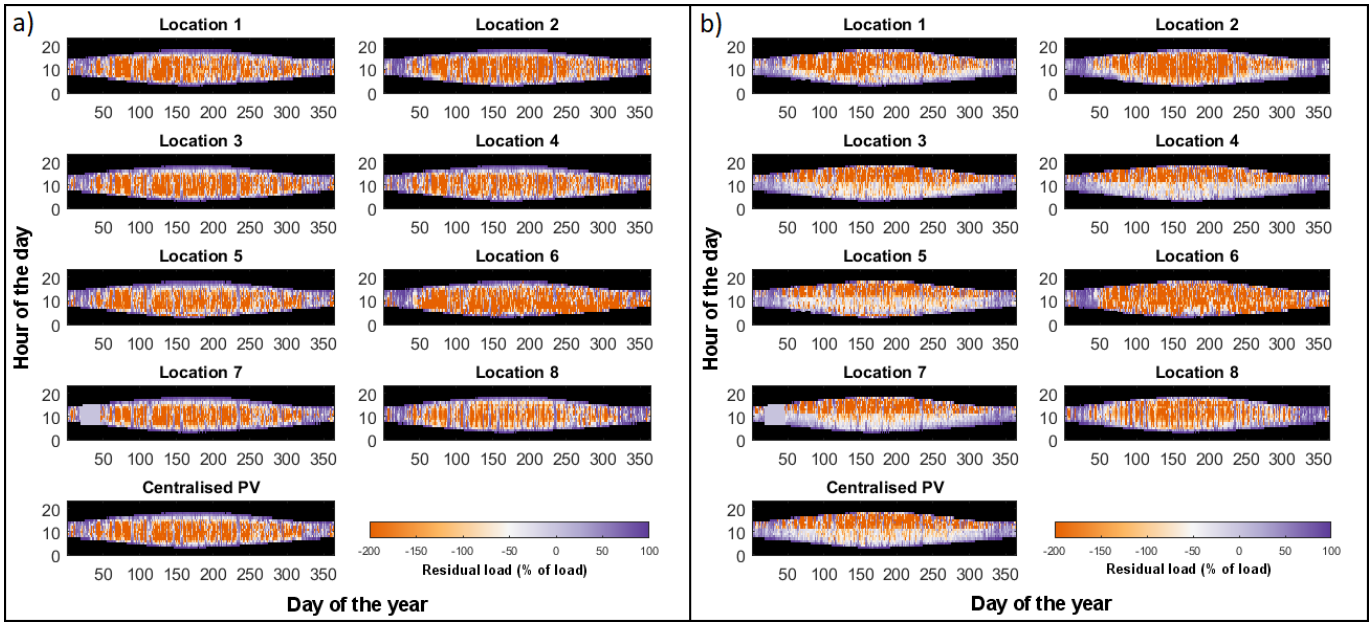

Fig. 8. CF optimized case (a) and SC optimized case (b) hourly RL for each location and centralized system

at Locations 1, 8, and 2. At Location 1, summer NRL decreases from –141.1% to –193.5%, at Location 8 drops from –236.0% to –279.1%, and at Location 2, it drops from –160.7% to –201.0%. These differences highlight how SC optimization can intensify overgeneration during peak irradiance periods. The centralized PV system shows a similar trend, with summer NRL decreasing from –108.9% in the CF optimized case to –147.1% in the SC optimized case. Figure 7b illustrates that RL dynamics in the SC optimized case are structurally similar to the CF optimized case, despite being optimized for a different objective.

An analysis at a deeper, hourly resolution across the entire year, which considered only hours where there was PV generation, reveals that in the CF optimized case, most locations experience frequent and widespread overgeneration during midday hours. This effect is especially pronounced in the summer period (days 150–250) when solar irradiance is the highest. Overproduction manifests as distinct bands of NRL, indicating that the PV systems are generating significantly more energy than can be consumed on-site during those hours. This pattern directly reflects the nature of CF optimization, which prioritizes maximizing the total energy yield over the course of the year. In doing so, it disregards the temporal alignment between generation and demand, resulting in surplus energy during periods of peak production, as shown in Fig. 8a. In Fig. 8, hourly demand and PV generation data were used to calculate RL for every hour of the year.

The hourly RL profiles for the SC optimized case have a different distribution compared to the CF optimized case, especially for Locations 3, 4, 5, 7, and the centralized PV system, where there is a pattern of NRL being closer to 0 at morning hours and more pronounced NRL at afternoon hours. This is the result of the PV system orientation to the west. For locations where the tilts of the PV system are lower, this pattern is less pronounced but still visible, as in the cases of Locations 1, 2, 6, and 8. At all locations, there are reduced extremes in RL visible, which were not visible in the daily resolution. These reduced extremes highlight the effectiveness of SC-oriented optimization in improving the temporal match between generation and demand. By focusing on alignment rather than maximizing total output, the SC case lowers energy shortfalls. The centralized PV setup also benefits, showing a less pronounced NRL and PRL during the entire year, as shown in Fig. 8b.

4.4. Positive residual load events

After the analysis of RL, the number of hours per year with PRL was calculated across all locations and the centralized PV system for both the CF and SC optimized cases. The differences are most pronounced at Locations 3, 5, and 6, where the CF optimized case has 162, 168, and 204 more PRL hours than the SC optimized case, respectively. This suggests that optimizing for capacity factor leads to longer periods of PV generation insufficient to meet the load, whereas the SC case better aligns production with consumption, reducing the frequency of supply deficits. Even the centralized PV system shows this pattern, with 1531 hours of PRL in the SC case versus 1704 in the CF case. Overall, the SC case offers improved self-sufficiency by minimizing the hours requiring external supply. In this study, resilience is considered in two distinct contexts: first, resilience to meteorological energy droughts, characterized by prolonged periods of low solar generation; and second, resilience to short-term supply disruptions or grid outages, where local generation adequacy and temporal alignment with demand are critical. The SC optimized case improves short-term supply adequacy by enhancing the temporal alignment between PV generation and demand, thereby reducing the frequency of PRL periods and minimizing reliance on external electricity during operational disruptions. This makes it particularly effective for maintaining an off-grid power supply in critical situations. Those events in

water supply systems can include [12]:

- Large-scale failures of electric power systems, which are called power blackouts, such as the recent example of the April 2025 blackout in Spain and Portugal.
- Extreme weather phenomena such as floods, for example, the 2024 Central European floods affecting the area where the analyzed water treatment facility is located.
- Cyberattack on IT systems, including automatic control of the water treatment process.
- Military conflicts, which are a rising concern amid the war crisis in the neighboring country, Ukraine.
- Failures of key water mains and pumping stations.

Conversely, the CF optimized case offers greater resilience against meteorological low-generation events (energy droughts). Although it results in a higher number of hours with PRL, the CF optimized case concentrates PV generation independently of the hourly demand shape. This is especially evident in Fig. 8a, where values reach substantially lower levels than in the SC optimized case for all hours when there is solar irradiance (Fig. 8b). This surplus provides a safety margin, allowing a larger share of the daytime electricity demand to be covered by PV generation even when solar irradiance is significantly reduced.

We also note that the findings in this study indicate that CF and SC optimization enhance different dimensions of system resilience and should not be interpreted as universally better strategies.

5. DISCUSSION AND CONCLUSIONS

In practical terms, the CF optimized case, which employs a tilt of about 34° and an azimuth of –6°, is the optimal PV system configuration for Locations 3, 4, 5, and 7 of the water treatment facility. A centralized PV system is a valid solution in the CF optimized case. For a centralized PV system installation in the CF optimized case, Location 5 is recommended. A centralized PV system in the CF optimized case maintains similar performance to decentralized systems while potentially simplifying operation and reducing costs. In the SC optimized centralized PV system, an increase in the SC rate of 2.76% compared to the CF-optimized case requires an increase in installed capacity from about 1.3 MWp to around 2.5 MWp, which is an increase of 1.2 MWp, illustrating the scale of the design trade-off. SC optimization results in PV systems that are west facing with tilt angles ranging from 10° to 90°. In the SC optimized case, locations that have a west-facing and steep-tilted PV system exhibit a great trade-off in CF (around 50%) for a slight increase of SC (around 2%). This trade-off is too great for practical implementation, as these PV system configurations require almost twice the capacity compared to CF optimized systems. In the SC optimized case, the centralized PV system faces the same issue, with a CF of only 6.93%, compared to 13.27% in the CF optimized case. After performing the RL analysis, the potential gain from west-facing, steep-tilted PV systems is still insufficient to make them a viable solution for Locations 3, 4, 5, and 7. However, for locations 1, 2, 6, and 8, where the tilt angles are lower, the CF values remain high enough (ranging from 10.16% to 11.57%) to consider the PV system configurations viable. Considering the RL analysis for these locations, the SC optimized PV system configuration is the preferred solution here. The analysis of PV system optimization in the water treatment facility reveals critical insights regarding the relationship between orientation parameters (azimuth and tilt angles), CF, and SC. Results for the CF optimized case from the MATLAB model agree with data from real PV systems in similar locations, such as that reported by Gulkowski [41]. The annual-scaling approach used in this study in equation (4) is a well-established baseline in both practice and literature [43–45]. The study highlights the trade-off between maximizing energy yield, as in the CF optimized case, and matching PV production to consumption patterns, as in the SC optimized case. CF optimization yields higher total energy but causes significant midday overgeneration and NRL. The SC optimization, which involves positioning PV arrays to better match the afternoon peak demand, reduces surplus generation at noon but shifts the overgeneration to afternoon hours and often requires larger system capacities due to inherently lower CF values. The lower yield in the SC optimized case for some locations, of around 50% of the initial CF optimized case, is consistent with what is stated by Fraunhofer ISE [46]. CF optimization consistently exhibits higher CF, but lower SC rates compared to the SC optimization scenario, which displays lower CF but improved SC ratios. SC ratios calculated in this paper are consistent with expected values. Bey *et al.* [9] state that a PV system can cover 53% of the electrical load of a water treatment plant, which is similar to the results reported in the present analysis. An example of a water utility with a PV array that supplies approximately 50% of its annual electricity demand, provided earlier in this paper, also underscores the validity of the results obtained in this study [23]. The Liu and Jordan model used in the PV generation model has some shortcomings, especially for azimuths over 15 degrees (or –15 degrees), and also for high PV module tilt angles [47]. Real-world data are scarce for PV modules installed westward (or eastward) at a tilt of 90 degrees in Europe, with only some data being available for building-integrated PV modules [48]. Experimental research for azimuths pointing more northward is also highly limited [49]. The PV generation model was evaluated by comparing its results with PVGIS data [50] for a 1 kWp system, applying identical 14% system losses. The Pearson correlation showed satisfactory agreement, as indicated in Table 4.

The RL analysis underscores the necessity of carefully balancing production and consumption to mitigate energy droughts and grid stress. These findings may inform future installations by highlighting the relevance of context-specific orientation strategies for improving environmental and economic performance in water treatment facilities. Furthermore, the occurrence of energy drought situations is a key consideration, both regarding localized energy shortages due to weather-related variability and broader system-wide challenges [51], which may be increasing in frequency, as suggested by recent studies [52]. Further research could include the analysis of energy costs for both the CF and SC optimized cases, such as the assessment of SC on water treatment energy costs shown by García-López *et al.* [53]. Additionally, the use of other renewable energy sources, such as wind turbines, is possible, as mentioned by Bartecka *et al.* [8].

Table 4
Pearson correlation coefficient of PV generation model data and PVGIS data

Location	CF optimized case	SC optimized case
1	1.00	0.99
2	0.99	0.99
3	0.99	0.97
4	0.99	0.98
5	0.99	0.97
6	1.00	0.99
7	0.99	0.97
8	0.99	0.99

Another approach is the consideration of energy storage. Also, an economic analysis considering energy spot prices is possible in this case. For PV modules with high tilt angles (90°) facing west, bifacial modules can be considered because they would capture both west- and eastward irradiation, as discussed in Reker *et al.* [54]. Another approach is to consider multi-oriented PV installations (split PV arrays), such as the east-west configurations discussed by Adua *et al.* [55]. As far as experimental research is concerned, more emphasis should be placed on researching PV module installation at high tilt angles and westward (or eastward) azimuths.

ACKNOWLEDGEMENTS

T. Liberski and J. Jurasz: This work documents the results of the research project no. 2022/47/B/ST8/01113 funded by the National Science Centre (Narodowe Centrum Nauki) titled: Method to quantify the energy droughts of renewable sources based on historical and climate change projections data.

F. A. Canales: The author would like to acknowledge the financial support received from the Polish National Agency for Academic Exchange (NAWA) under the Ulam NAWA Programme (Agreement no. BPN/ULM/2022/1/00092/U/00001). Fausto A. Canales also thanks Universidad Militar Nueva Granada for its support, as this product is part of his academic work as a professor at this institution.

The authors are grateful to Mikołaj Ostraszewski for his careful proofreading of the final version of the manuscript and for valuable comments that improved its clarity.

DATA AVAILABILITY

The data and MATLAB scripts supporting the findings of this study are openly available in Zenodo at https://doi.org/10.5281/zenodo.18240766

REFERENCES

[1] K. Świętochowski, M. Świętochowska, M. Kalenik, and J. Gwoździej-Mazur, "Analysis of the Use of a Low-Power Photovoltaic System to Power a Water Pumping Station in a Tourist Town," *Energies*, vol. 16, no. 21, p. 7435, Nov. 2023, doi: 10.3390/en16217435.

[2] H.E. Chabour, M.A. Pardo, and A. Riquelme, "Economic assessment of converting a pressurised water distribution network into an off-grid system supplied with solar photovoltaic energy," *Clean Technol. Environ. Policy*, vol. 24, no. 6, pp. 1823–1835, Aug. 2022, doi: 10.1007/s10098-022-02290-5.

[3] M. Kacprzak, K. Ramm, and G. Wiśniewski, *Energy Efficiency in Water and Wastewater Utilities*. Polish Chamber of Waterworks and Sewerage, 2019. [Online]. Available: https://www.igwp.org.pl/wydawnictwa/efektywnosc-energetyczna-w-przedsiebiorstwach-wodociagowo-kanalizacyjnych/

[4] C. Douville and J. Macknick, "Energy Usage and Management at a Large Wastewater Treatment Facility in Boulder, Colorado," in *ASME 2011 International Mechanical Engineering Congress and Exposition (IMECE 2011)*, Denver, USA, Nov. 2011, pp. 653–659. doi: 10.1115/IMECE2011-65994.

[5] Q. Zhao, W. Wu, J. Yao, A.R. Simpson, A. Willis, and L. Aye, "Sizing behind-the-meter solar PV for pumped water distribution systems: A comparison of methods," *J. Clean Prod.*, vol. 434, p. 140210, Jan. 2024, doi: 10.1016/j.jclepro.2023.140210.

[6] A. Stawowy, R. Wrona, M. Sawczuk, and D. Lasek, "Profitability of Photovoltaic and Energy Storage System in a Foundry Plant," *Arch. Foundry Eng.*, vol. 23, no. 2, pp. 100–105, 2023, doi: 10.24425/afe.2023.144300.

[7] M.C. Collivignarelli *et al.*, "Disinfection of wastewater by uv-based treatment for reuse in a circular economy perspective. Where are we at?," *Int. J. Environ. Res. Public Health*, vol. 18, p. 77, Dec. 2020, doi: 10.3390/ijerph18010077.

[8] M. Bartecka, P. Terlikowski, M. Kłos, and Ł. Michalski, "Sizing of prosumer hybrid renewable energy systems in Poland," *Bull. Pol. Acad. Sci. Tech. Sci.*, vol. 68, no. 4, pp. 721–731, Aug. 2020, doi: 10.24425/bpasts.2020.133125.

[9] M. Bey, A. Hamidat, and T. Nacer, "Eco-energetic feasibility study of using grid-connected photovoltaic system in wastewater treatment plant," *Energy*, vol. 216, p. 119217, Feb. 2021, doi: 10.1016/j.energy.2020.119217.

[10] M. Rumbayan, I. Pundoko, S.R. Sompie, and D.G. Ruindungan, "Integration of smart water management and photovoltaic pumping system to supply domestic water for rural communities," *Results Eng.*, vol. 25, p. 103966, Mar. 2025, doi: 10.1016/j.rineng.2025.103966.

[11] Q. Shao *et al.*, "Low-carbon scheduling of electricity consumption in wastewater treatment plant by using photovoltaic system," *Sci. Total Environ.*, vol. 933, p. 173062, Jul. 2024, doi: 10.1016/j.scitotenv.2024.173062.

[12] D. Szpak, B. Tchórzewska-Cieślak, and M. Stręk, "A New Method of Obtaining Water from Water Storage Tanks in a Crisis Situation Using Renewable Energy," *Energies*, vol. 17, no. 4, p. 874, Feb. 2024, doi: 10.3390/en17040874.

[13] B. Sreewirote, N. Suttisinthong, and A. Ngaopitakkul, "The Application of Solar Cells for Water Filtration System," *MATEC Web Conf.*, vol. 260, p. 03002, 2019, doi: 10.1051/matecconf/201926003002.

[14] E. Kazanecka and P. Olczak, "A specific yield comparison of 2 photovoltaic installations – Polish case study," *Polityka Energetyczna*, vol. 26, no. 4, pp. 129–148, 2023, doi: 10.33223/epj/171857.

[15] P. Borah, L. Micheli, and N. Sarmah, "Analysis of Soiling Loss in Photovoltaic Modules: A Review of the Impact of Atmospheric Parameters, Soil Properties, and Mitigation Approaches," *Sustainability*, vol. 15, p. 16669, 2023, doi: 10.3390/su152416669.

[16] M. Jaszczur *et al.*, "The field experiments and model of the natural dust deposition effects on photovoltaic module efficiency," *Environ. Sci. Pollut. Res.*, vol. 26, no. 9, pp. 8402–8417, Mar. 2019, doi: 10.1007/s11356-018-1970-x.

[17] J. Cano, J.J. John, S. Tatapudi, and G.S. TamizhMani, *Effect of Tilt Angle on Soiling of Photovoltaic Modules*. IEEE, 2014. doi: 10.1109/PVSC. 2014.6925610.

[18] F. Kaspar, M. Borsche, U. Pfeifroth, J. Trentmann, J. Drücke, and P. Becker, "A climatological assessment of balancing effects and shortfall risks of photovoltaics and wind energy in Germany and Europe," in *Advances in Science and Research*, Copernicus Publications, Jul. 2019, pp. 119–128. doi: 10.5194/asr-16-119-2019.

[19] C. González-Morán, P. Arboleya, and V. Pilli, "Photovoltaic self consumption analysis in a European low voltage feeder," *Electr. Power Syst. Res.*, vol. 194, p. 107087, May 2021, doi: 10.1016/j.epsr.2021.107087.

[20] E. Nyholm, J. Goop, M. Odenberger, and F. Johnsson, "Solar photovoltaic-battery systems in Swedish households – Self-consumption and self-sufficiency," *Appl. Energy*, vol. 183, pp. 148–159, Dec. 2016, doi: 10.1016/j.apenergy.2016.08.172.

[21] S. Pater, "Increase of energy self-consumption in hybrid RES installations with PV panels and air-source heat pumps," *Chem. Process Eng.-New Front.*, vol. 44, no. 4, p. e43, 2023, doi: 10.24425/cpe.2023.147402.

[22] G. Cillari, F. Fantozzi, and A. Franco, "Monitoring of photovoltaic systems and evaluation of building energy self-consumption," in *J. Phys.-Conf. Ser.*, vol. 2042, p. 012088, Nov. 2021. doi: 10.1088/1742-6596/2042/1/012088.

[23] Gramwzielone.pl, "More Water and Energy from Own Sources at Chrzanow Waterworks," May 2024. [Online]. Available: https://www.gramwzielone.pl/energia-sloneczna/20314758/coraz-wiecej-wody-i-energii-z-wlasnych-zrodel-w-wodociagach-chrzanowskich

[24] K. van der Wiel, L.P. Stoop, B.R.H. van Zuijlen, R. Blackport, M.A. van den Broek, and F.M. Selten, "Meteorological conditions leading to extreme low variable renewable energy production and extreme high energy shortfall," *Renew. Sustain. Energy Rev.*, vol. 111, pp. 261–275, Sep. 2019, doi: 10.1016/j.rser.2019.04.065.

[25] M. Schlemminger, D. Bredemeier, A. Mahner, R. Niepelt, M.H. Breitner, and R. Brendel, "Storage requirments in urban energy systems for the integration of rooftop photovoltaics," in Proc. *International Renewable Energy Storage and Systems Conference (IRES 2023),* 2024, pp. 28–36. doi: 10.2991/978-94-6463-455-6_5.

[26] M. Ohba, Y. Kanno, and S. Bando, "Effects of meteorological and climatological factors on extremely high residual load and possible future changes," *Renew. Sustain. Energy Rev.*, vol. 175, p. 113188, Apr. 2023, doi: 10.1016/j.rser.2023.113188.

[27] U. Pfeifroth, J. Trentmann, R. Hollmann, and P. Fuchs, "Surface Solar Radiation Data Set – Heliosat (SARAH) – Edition 3," *Satellite Application Facility on Climate Monitoring (CM SAF)*, 2020, doi: 10.5676/EUM_SAF_CM/SARAH/V003.

[28] H. Hersbach *et al.*, "The ERA5 global reanalysis," *Q. J. R. Meteorolog. Soc.*, vol. 146, no. 730, pp. 1999–2049, 2020, doi: 10.1002/qj.3803.

[29] J.A. Duffie, W.A. Beckman, and N. Blair, *Solar Engineering of Thermal Processes, Photovoltaics and Wind*, 5th edition. Wiley, 2020.

[30] T. Ruan, F. Wang, M. Topel, B. Laumert, and W. Wang, "A new optimal PV installation angle model in high-latitude cold regions based on historical weather big data," *Appl. Energy*, vol. 359, Apr. 2024, p. 122690, doi: 10.1016/j.apenergy.2024.122690.

[31] S. Soulayman, "Comments on solar azimuth angle," *Renew. Energy*, vol. 123, pp. 294–300, Aug. 2018, doi: 10.1016/j.renene.2018.02.063.

[32] M. Gulin, M. Vašak, and M. Baotic, "Estimation of the global solar irradiance on tilted surfaces," in *17th International Conference on Electrical Drives and Power Electronics (EDPE 2013)*, Dubrovnik, Croatia, Jan. 2013, pp. 334–339. [Online]. Available: www.lares.fer.hr

[33] B.Y.H. Liu and R.C. Jordan, "The Interrelationship and of Direct, Diffuse and Characteristic Distribution Total Solar Radiation," *Solar Energy*, vol. 4, no. 3, pp. 1–19, 1960, doi: 10.1016/0038-092X(60)90062-1.

[34] D.L. King, W.E. Boyson, and J.A. Kratochvill, "Photovoltaic Array Performance Model," Sandia National Laboratories Report, Dec. 2004. doi: 10.2172/919131.

[35] S. Gulkowski, "Modeling and Experimental Studies of the Photovoltaic System Performance in Climate Conditions of Poland," *Energies*, vol. 16, no. 20, p. 7017, Oct. 2023, doi: 10.3390/en16207017.

[36] A.H. Duhis, M. Aljanabi, and M.S.S. Al-Kafaji, "Increasing photovoltaic system power output with white paint albedo – a scenario in Al-Mausaib City using PVSyst. software," *Int. J. Power Electron. Drive Syst.*, vol. 14, no. 2, pp. 1149–1159, Jun. 2023, doi: 10.11591/ijpeds.v14.i2.pp1149-1159.

[37] B.H. King, C.D. Robinson, C. Carmignani, D. Riley, and C.B. Jones, "Application of the Sandia Array Performance Model to Assess Multiyear Performance of Fielded CIGS PV Arrays," in *2018 IEEE 7th World Conference on Photovoltaic Energy Conversion (WCPEC) (A Joint Conference of 45th IEEE PVSC, 28th PVSEC & 34th EU PVSEC)*, 2018, pp. 3607–3612. doi: 10.1109/PVSC.2018.8548108.

[38] B.H. King, C.W. Hansen, D. Riley, C.D. Robinson, and L. Pratt, "Outdoor test and analysis procedures for generating coefficients for the Sandia Array Performance Model," in *2016 IEEE 43rd Photovoltaic Specialists Conference (PVSC)*, 2016, pp. 3051–3056. doi: 10.1109/PVSC.2016.7750225.

[39] S.F.A. Shah, I.A. Khan, and H.A. Khan, "Performance Evaluation of Two Similar 100MW Solar PV Plants Located in Environmentally Homogeneous Conditions," *IEEE Access*, vol. 7, pp. 161697–161707, 2019, doi: 10.1109/ACCESS.2019.2951688.

[40] J. Jurasz, J. Mikulik, P.B. Dabek, M. Guezgouz, and B. Kaźmierczak, "Complementarity and 'Resource Droughts' of Solar and Wind Energy in Poland: An ERA5-Based Analysis," *Energies*, vol. 14, no. 4, p. 1118, Feb. 2021, doi: 10.3390/en14041118.

[41] S. Gulkowski, "Specific Yield Analysis of the Rooftop PV Systems Located in South-Eastern Poland," *Energies*, vol. 15, no. 10, p. 3666, May 2022, doi: 10.3390/en15103666.

[42] D.C. Jordan and S.R. Kurtz, "Photovoltaic degradation rates – An Analytical Review," *Prog. Photovolt-Res. Appl*, vol. 21, pp. 12–29, Jan. 2013, doi: 10.1002/pip.1182.

[43] I. Suarez-Ramon, M. Alvarez-Rodriguez, C. Ruiz-Manso, F. Perez-Dominguez, and P. Gonzalez-Vega, "A general sizing methodology of grid-connected PV systems to meet the zero-energy goal in buildings," *Energy*, vol. 306, p. 132580, Oct. 2024, doi: 10.1016/J.ENERGY.2024.132580.

[44] N. Li, Z. Lukszo, and J. Schmitz, "An approach for sizing a PV–battery–electrolyzer–fuel cell energy system: A case study at a field lab," *Renew. Sustain. Energy Rev.*, vol. 181, p. 113308, Jul. 2023, doi: 10.1016/J.RSER.2023.113308.

[45] "Annual Yield – PV Performance Modeling Collaborative (PVPMC)." Accessed: Dec. 23, 2025. [Online]. Available: https://pvpmc.sandia.gov/modeling-guide/5-ac-system-output/pv-performance-metrics/annual-yield/

[46] H. Wirth and S.B. Judith, "Recent Facts about Photovoltaics in Germany." [Online]. Available: www.pv-fakten.de

[47] G. Li, Y. Yang, and R. Tang, "On the estimation of daily beam radiation on tilted surfaces," in *2011 International Conference on Electrical and Control Engineering, ICECE 2011 – Proc.*, 2011, pp. 3552–3555. doi: 10.1109/ICECENG.2011.6058344.

[48] B. Dragsted and S. Svendsen, "Building-integrated photovoltaics facade test site data, 2022/2023," 2023, DTU Data. doi: 10.11583/DTU.24745329.v1.

[49] H.Y. Cheng, C.C. Yu, K.C. Hsu, C.C. Chan, M.H. Tseng, and C.L. Lin, "Estimating Solar Irradiance on Tilted Surface with Arbitrary Orientations and Tilt Angles," *Energies*, vol. 12, no. 8, p. 1427, Apr. 2019, doi: 10.3390/en12081427.

[50] T. Huld, R. Müller, and A. Gambardella, "A new solar radiation database for estimating PV performance in Europe and Africa," *Solar Energy*, vol. 86, no. 6, pp. 1803–1815, 2012, doi: 10.1016/j.solener.2012.03.006.

[51] M. Li *et al.*, "Renewable energy quality trilemma and coincident wind and solar droughts," *Commun. Earth Environ.*, vol. 5, no. 1, p. 661, Dec. 2024, doi: 10.1038/s43247-024-01850-5.

[52] J. Kapica *et al.*, "The potential impact of climate change on European renewable energy droughts," *Renew. Sustain. Energy Reviews*, vol. 189, p. 114011, Jan. 2024, doi: 10.1016/J.RSER.2023.114011.

[53] M. García-López, B. Montano, and J. Melgarejo, "The Influence of Photovoltaic Self-Consumption on Water Treatment Energy Costs: The Case of the Region of Valencia," *Sustainability*, vol. 15, no. 15, p. 1508, Aug. 2023, doi: 10.3390/su151511508.

[54] S. Reker, J. Schneider, and C. Gerhards, "Integration of vertical solar power plants into a future German energy system," *Smart Energy*, vol. 7, p. 100083, Aug. 2022, doi: 10.1016/j.segy.2022.100083.

[55] E. Abba Muhammad Adua, "Comparisons of east/west and south oriented photovoltaic (PV) systems in terms of performance and land utilization with the best optimum tilt angles," *Int. Res. J. Modernization Eng. Technol. Sci.*, vol. 5, pp. 2582–5208, Sep. 2023, [Online]. Available: https://www.irjmets.com/uploadedfiles/paper//issue_8_august_2023/44027/final/fin_irjmets1694369231.pdf